Springer

Available online at https://link.springer.com
http://www.jhydrod.com/
2018,30(1):106-113
https://doi.org/10.1007/s42241-018-0011-z

SPH numerical investigation of the characteristics of an oscillating hydraulic jump at an abrupt drop*

Diana De Padova [1], Michele Mossa [1], Stefano Sibilla [2]
1. *Department of Civil, Environmental Land, Building Engineering and Chemistry, Polytechnic University of Bari, Bari 70125, Italy*
2. *Department of Civil Engineering and Architecture, University of Pavia, Pavia, 27100, Italy*

(Received October 31, 2017, Accepted December 14, 2017)

Abstract: This paper shows the results of the smooth particle hydrodynamics (SPH) modelling of the hydraulic jump at an abrupt drop, where the transition from supercritical to subcritical flow is characterised by several flow patterns depending upon the inflow and tailwater conditions. SPH simulations are obtained by a pseudo-compressible XSPH scheme with pressure smoothing; turbulent stresses are represented either by an algebraic mixing-length model, or by a two-equation k-ε model. The numerical model is applied to analyse the occurrence of oscillatory flow conditions between two different jump types characterised by quasi-periodic oscillation, and the results are compared with experiments performed at the hydraulics laboratory of Bari Technical University. The purpose of this paper is to obtain a deeper understanding of the physical features of a flow which is in general difficult to be reproduced numerically, owing to its unstable character: in particular, vorticity and turbulent kinetic energy fields, velocity, water depth and pressure spectra downstream of the jump, and velocity and pressure cross-correlations can be computed and analysed.

Key words: Hydraulic jumps, smoothed particle hydrodynamics (SPH) models, oscillating characteristics

Introduction

At an abrupt drop the transition from supercritical to subcritical flow is characterised by several flow patterns depending upon the inflow and tailwater flow conditions. Figure 1 summarises well acknowledged flow patterns.

Some researchers pointed out the existence of oscillating phenomena[2-5]. These oscillating characteristics can consist of: (1) change from one type of hydraulic jump to another, (2) horizontal movement of the jump toe, (3) cyclic variation of velocity components and pressure in the region close to the jump roller, (4) formation, development and coalescence of large-scale flow structures.

As shown by Ref. [6], specific flow conditions can lead to cyclic oscillations between jump types, resulting in the cyclic formation and evolution of jump vortices.

Meshless Lagrangian techniques appear to be particularly suitable to represent the complex and highly-unsteady free-surface patterns which characterize a hydraulic jump: a number of realizations obtained with smoothed particle hydrodynamics (SPH) have shown that this method can be successfully applied to the simulation of standing waves[7-9], of wave trains issuing from flapping jets[10], of hydraulic jumps[11-14] and of spilling breakers[15], being able to reproduce, both qualitatively and quantitatively, their average and time-dependent features.

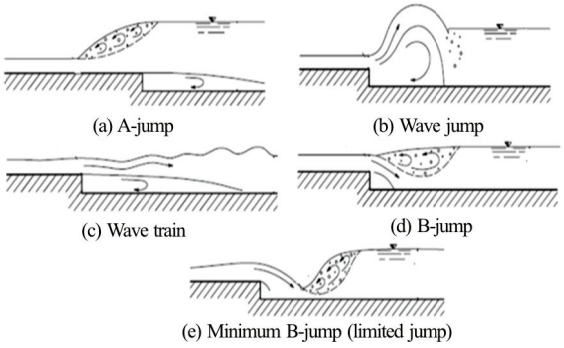

Fig. 1 Flow conditions (from Ohtsu and Yasuda[1])

The purpose of this paper is therefore to use a

* **Biography:** Diana De Padova (1981-), Female, Ph. D., Research Assistant
Corresponding author: Diana De Padova,
E-mail: diana.depadova@poliba.it

weakly-compressible SPH (WCSPH) scheme, together with a suitable turbulence model, to study the oscillating characteristics and cyclic mechanisms which can occur in a hydraulic jump at an abrupt drop in certain conditions, leading to an alternate shift of the flow pattern between the B-jump and the wave jump.

The numerical results are eventually compared to the laboratory experiments by Mossa et al.[6], in order to obtain a deeper understanding of the physical features of this particular kind of unsteady flow.

1. Experimental setup

Experimental investigations were carried out in the laboratory of the Civil and Environmental Engineering Department-Water Engineering Division (hereafter referred to as SIA) of Bari Polytechnic University in a 0.4 m wide, 24.4 m long channel (with sidewalls 0.5 m height). The walls and bottoms of both channels were made of Plexiglas (Fig. 2). The channel hosted in recent years widespread experimental activity on hydraulic jump characterization[4, 6, 16-19].

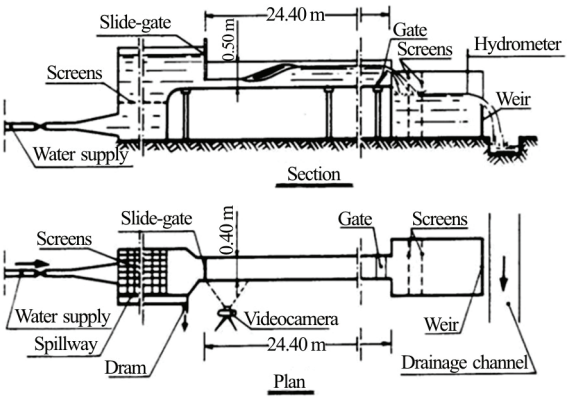

(a) Sketch

(b) Picture of the channel

Fig. 2 (Color online) Channel at the hydraulic laboratory of the laboratory of the Civil and Environmental Engineering Department-Water Engineering Division of Bari Polytechnic University

Table 1 Parameters of the analysed oscillating hydraulic jump

Run no. Mossa et al.[6]	B32
y_1/mm	35.0
y_t/mm	166.3
V_1/ms^{-1}	1.93
V_t/ms^{-1}	0.40
F_1/mm	33.0
y_1 / y_t	4.75
s	3.20
Jump type	B-wave

In the SIA channel, the abrupt drop was made of Plexiglas and located 0.8 m downstream of the gate. The tested elevation drops were equal to 32.0 mm or 65.2 mm. Discharges were measured by a triangular sharp-crested weir. Measurements of upstream and downstream water depths were carried out with electric hydrometers type point gauges supplied with electronic integrators, which yielded directly the estimate of the time-averaged flow depth. The hydrometers, supplied with verniers, had a measurement accuracy of ± 0.1 mm. Water discharge and tailwater depth were regulated by two gates placed, respectively, at the upstream and downstream ends of the channel. For some runs, pressure measurements under the jumps were obtained using a pressure transducer type 4 310 of Society TransInstruments with a relative pressure difference range equal to 0 Pa-7 500 Pa.

The pressure tap was connected to the transducer using a rigid tube with 2 .0 mm diameter and 0.4 m of length. An amplifier and a conditioner were used to adjust the signal output of the transducer for resolution and acceptable range of the A/D board. In addition, a videocamera was used to film the jump for some runs.

Table 1 lists the main experimental parameters of the investigated hydraulic jump: y_1 is the inflow water depth, y_t is the water depth downstream of the jump, $F_1 = V_1 (g y_1)^{0.5}$ is the inflow Froude number and Re is the Reynolds number defined as $Re = V_1 y_1 / \nu = V_t y_t / \nu$ where V_1 and V_t are the flow velocities at the water depths y_1 and y_t, respectively, and ν is the kinematic water viscosity at the run temperature.

2. SPH numerical method

SPH simulations were obtained by a code developed at the Fluid Mechanics Laboratory of the Department of Civil Engineering and Architecture of the University of Pavia. The code solves the Navier-Stokes equations with a standard weakly compressible

SPH (WCSPH) scheme[20, 21], where a reduced compressibility modulus of 10^6 Pa is assumed for water and a pressure smoothing procedure is applied at every time step to the difference between local and hydrostatic pressure in order to reduce the numerical noise in pressure evaluation[11].

A renormalization procedure for the SPH kernel approximation is applied to enforce consistency on the numerical estimate of the derivatives in the velocity and stress divergence terms[22].

An algebraic mixing-length model and a two-equation model were tested to represent turbulent stresses. The mixing-length model is based on the introduction of a mixing-length $l_m = f_i \min(\kappa z, l_{\max})$, where $\kappa = 0.41$ is the Von Kármán constant, z is the distance from the wall, $l_{\max}$ is a cutoff maximum value and

$$f_i = \min\left[1, \left|\sum_j \frac{m_j}{\rho_j}\nabla W_{ij}\right|^{-3}\right] \tag{1}$$

is a damping function which is less than unity only near the free surface. The effect of f_i is to bound 1.0 m near the free surface, where a non-physical growth of the eddy viscosity may lead to numerical instabilities[23, 24].

The two-equation model is a SPH version of the Standard k-ε turbulence model[25]:

$$\frac{\mathrm{D}k_i}{\mathrm{D}t} = P_{k_i} + \frac{1}{\sigma_k}\sum_j m_j \frac{\nu_{T_i} + \nu_{T_j}}{\rho_i + \rho_j}\frac{k_i - k_j}{r_{ij}^2 + 0.01b^2}\boldsymbol{r}_{ij}\cdot\nabla W_{ij} - \varepsilon_i \tag{2a}$$

$$\frac{\mathrm{D}\varepsilon_i}{\mathrm{D}t} = \frac{1}{\sigma_\varepsilon}\sum_j m_j \frac{\nu_{T_i} + \nu_{T_j}}{\rho_i + \rho_j}\frac{\varepsilon_i - \varepsilon_j}{r_{ij}^2 + 0.01b^2}\boldsymbol{r}_{ij}\cdot\nabla W_{ij} + C_{\varepsilon_1}\frac{\varepsilon_i}{k_i}P_{k_i} + C_{\varepsilon_2}\frac{\varepsilon_i}{k_i}\sum_j \frac{m_j}{\rho_j}\varepsilon_j W_{ij} \tag{2b}$$

where P_k is the production of turbulent kinetic energy depending on the local rate of deformation, ν_T is the eddy viscosity and $\sigma_k = 1.0$, $\sigma_\varepsilon = 1.3$, $C_{\varepsilon_1} = 1.44$ and $C_{\varepsilon_2} = 1.92$ are model constants whose values are those proposed for the standard k-ε formulation.

The k and ε values at the inflow are computed by assuming a constant 5% turbulence intensity and a mixing length equal to $0.5y_1$.

According to the standard XSPH approach, at each time step a new particle velocity $\boldsymbol{v}^T$ is obtained by explicit integration of the momentum Eq. (2) while a smoothed value of velocity $\boldsymbol{v}^s$ is obtained by

$$\boldsymbol{v}^s(\boldsymbol{x}_i) = (1-\varphi)\boldsymbol{v}^T(\boldsymbol{x}_i) + \varphi\frac{\sum_j \frac{m_j}{\rho_j}\boldsymbol{v}^T(\boldsymbol{x}_j)W_{ij}}{\sum_j \frac{m_j}{\rho_j}W_{ij}} \tag{3}$$

and used for particle movement. The smoothing parameter φ controls the intensity of velocity filtering.

3. Numerical test and results

The SPH 2-D simulation of the hydraulic jump reported in Table 1, wasperformed in a physical domain consisting in a rectangle 2.0 m long and 0.4 m high, shorter than the real channel in the test facility. The shorter domain was chosen in order to reduce the computational cost without influencing the quality of the numerical solution.

A schematic figure of the problem setup can be seen in Fig. 3.

Fig. 3 (Color online) Schematic figure of the geometrical setup. Solid black lines indicates solid walls, dashed blue lines the initial free surface and dashed red lines show the position of the inflow and outflow boundaries

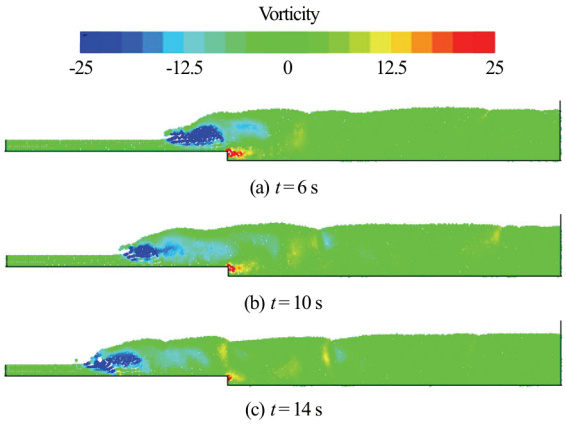

Fig. 4 (Color online) Instantaneous SPH vorticity fields in the SPH simulation with a velocity smoothing coefficient φ equal to 0.005. Vorticity values in the color scale are expressed in s^{-1}

The SPH simulation of the experimental test on hydraulic jump was performed by adopting a velocity smoothing coefficient in the XSPH scheme $\varphi =$

0.010: a sensitivity analysis showed that the simulations with either a higher ($\varphi = 0.020$) or a lower ($\varphi = 0.005$) velocity smoothing coefficient were not able to reproducethe oscillating characteristics and cyclic mechanisms of this hydraulic jump (Figs. 4, 5). A value $\varphi = 0.010$ guarantees instead the stability of the SPH solutions without affecting the quality of the numerical results.

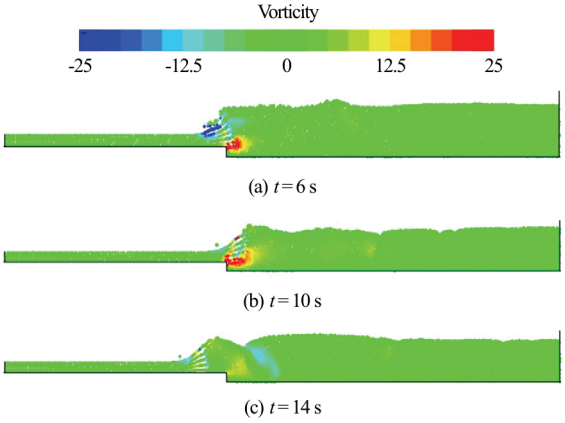

Fig. 5 (Color online) Instantaneous SPH vorticity fields in the SPH simulation with a velocity smoothing coefficient φ equal to 0.02. Color scale as in Fig. 4

Table 2 Numerical parameters of the SPH simulations in the sensitivity analysis

Test	Turbulence mdel	η/Σ	N_p
T1a	Mixing -length model	1.5	3 000
T1b	k-ε turbulence model	1.5	3 000

The simulation of the hydraulic jump test case was performed by adopting either the mixing length turbulence model with $l_{\max} = 0.5h_2$ (test T1a) or the two-equation k-ε model (2) (test T1b). Some of the results are here summarized. Table 2 lists the principal characteristics of the two SPH simulations.

The ratio of the smoothing length to the initial particle spacing Σ, which influences the efficiency of the SPH kernel function[26], was maintained to a constant value of $\eta/\Sigma = 1.5$ [27]. The obtained SPH results show that an initial particle spacing $\Sigma \leq 0.01$ m guarantees the onset of the hydraulic jump oscillations and yields a result in accordance with the experiments (Figs. 6-9).

The sensitivity analysis is here shown for test T1b, and shows that the vorticity field is predicted quite accurately even by the coarsest resolution, although some detail is lost in the middle of the roller (Figs. 6 and 8).

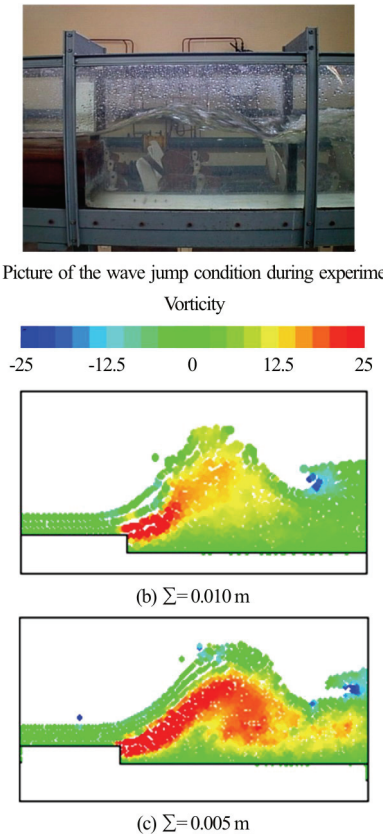

Fig. 6 (Color online) Instantaneous SPH vorticity fields (t = 8 s) in the SPH simulation (Test T1b) with different particle resolutions. Color scale as in Fig. 4

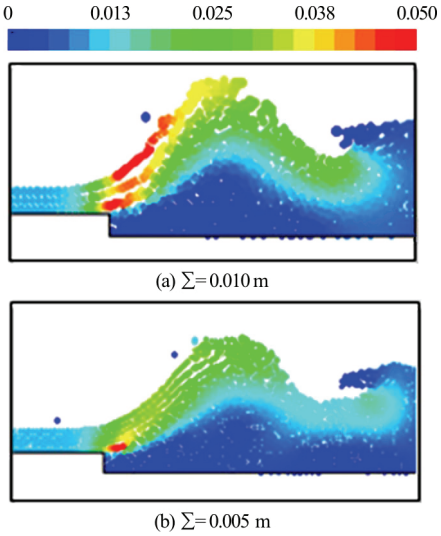

Fig. 7 (Color online) Instantaneous SPH turbulent kinetic energy fields (wave jump condition: t = 8 s) in the SPH simulation (Test T1b) with different particle resolutions. Turbulent kinetic energy values in the color scale are expressed in m^2s^{-2}

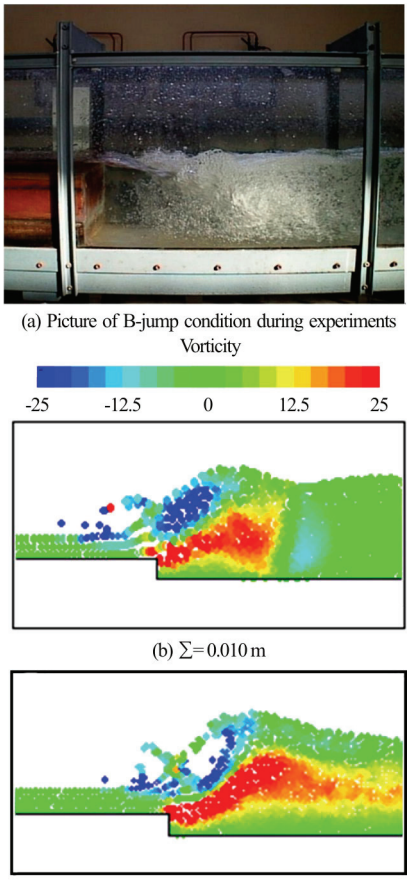

Fig. 8 (Color online) Instantaneous SPH vorticity fields (t = 12 s) in the SPH simulation (Test T1b) with different particle resolutions. Color scale as in Fig. 4

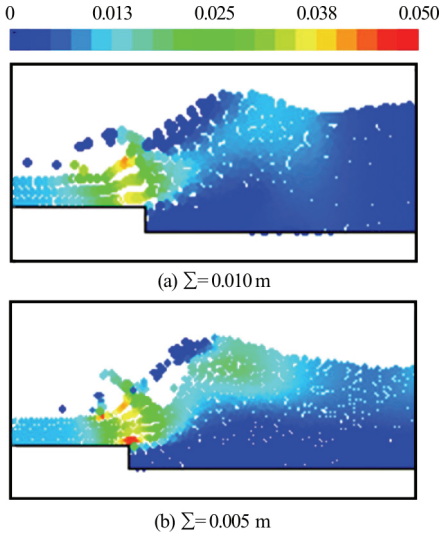

Fig. 9 (Color online) Instantaneous SPH turbulent kinetic energy fields (B-jump condition: t = 12 s) in the SPH simulation (Test T1b) with different particle resolutions. Color scale as in Fig. 4

The turbulent kinetic energy fields are also similar, although an overprediction of k near the surface occurs near the surface in the wave-jump phase of the oscillation, when the coarser resolutionis applied (Fig. 7).

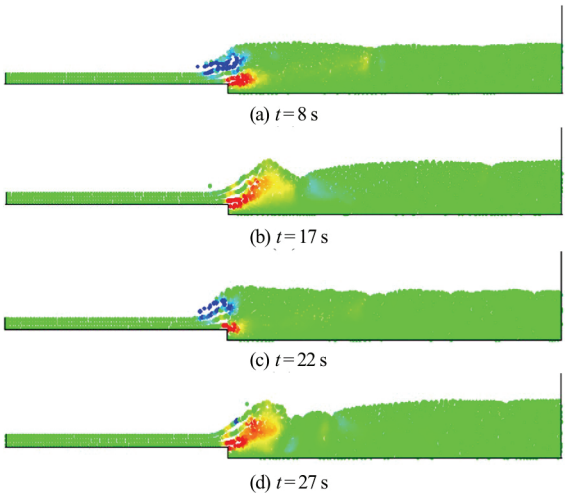

Fig. 10 (Color online) Instantaneous SPH vorticity fields in the SPH simulation of Test T1a

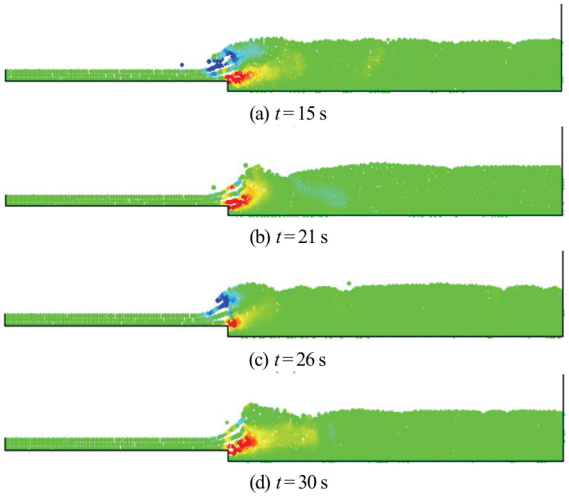

Fig. 11 (Color online) Instantaneous SPH vorticity fields in the SPH simulation of Test T1b

The results of both SPH simulations were employed to analyze the details of the oscillations between the different jump types. The analysis was useful to study the cyclic formation and evolution of the jump vortices. Both the mixing length model and the k - ε model yield similar results and are able to predict the oscillating characteristics and cyclic mechanisms in hydraulic jumps.

The instantaneous vorticity fields (Figs. 10(a)-11(d)) of the configuration with oscillations between the B and wave jump clearly indicate that the transi-

tion phase between the two jump types is well reproduced by both turbulence models (T1a and T1b). Vortices are characterized by a clockwise or anti-clockwise rotation, depending on which type of jump is present. In particular, vortices are characterized by a clockwise rotation when the wave jump occurs (Figs. 10(b)-10(d) and Figs. 11(b)-11(d)) and by an anti-clockwise one for the B jump (Figs. 10(a)-10(c) and Figs. 11(a)- 11(c)), respectively.

As previously shown, the T1b simulation with the k-ε turbulence model is also able to show that the highest levels of turbulent energy are always found at the jump toe (Figs. 7 and 9), but turbulence appears to be more persistent in the wave-jump phase of the oscillation, when a sub-surface turbulent layer flows downstream along the wave jump (Fig. 7).

Figure 12 show the amplitude spectrum of the pressure fluctuations computed in tests T1a and T1b, compared with the measurements under the hydraulic jump B32 of Table 1, where the pressure tap was located at a distance of 0.26 m from the time-averaged position of the jump toe.

From the analysis of the spectrum it is clear that even the pressure fluctuations are quasi-periodic and strongly influenced by the oscillations between the B and wave jump types; furthermore, it is possible to observe the existence of a peak in each spectrum, as it was shown in the experiments by Mossa et al.[6].

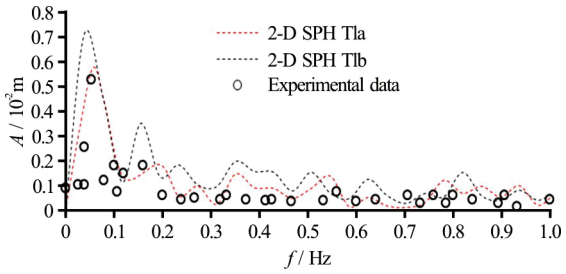

Fig. 12 (Color online) Amplitude spectrum of pressure fluctuations under hydraulic jump (configuration B32 of Table 1) for the SPH simulations of test T1 and two different turbulence models: mixing-length (T1a) and k-ε (T1b)

Although both turbulence models yield similar results, the detailed comparison of the computed amplitude spectra with the measured ones shows that the results obtained with the mixing-length model are closer to the experimental data than the k-ε ones (Fig. 12). The peak frequency is slightly higher than 0.1 Hz for test T1a, as shown by[6], while it is lower than 0.1 Hz for test T1b.

Figures 13(a)-13(c) show a part of the time series of the pressure p, of the horizontal (u) and of the vertical (v) velocity components, computed at the bottom under the hydraulic jump T1a of Table 2, near the time-averaged position of the hydraulic jump toe.

From the analysis of the Figs. 13(a)-13(c), it is clear that velocity components and pressure fluctuations, are strongly influenced by the oscillations between the B and wave jump types. The time histories (Fig. 13(a)) show that low pressures (low water depths) can be correlated with the horizontal flow upstream of the wave-jump, while higher pressures (and depths) can be correlated with the upward flow caused by the roller in the B-jump phase. Therefore, the analysis of the oscillating phenomena indicates a correlation among the velocity components and pressure fluctuations.

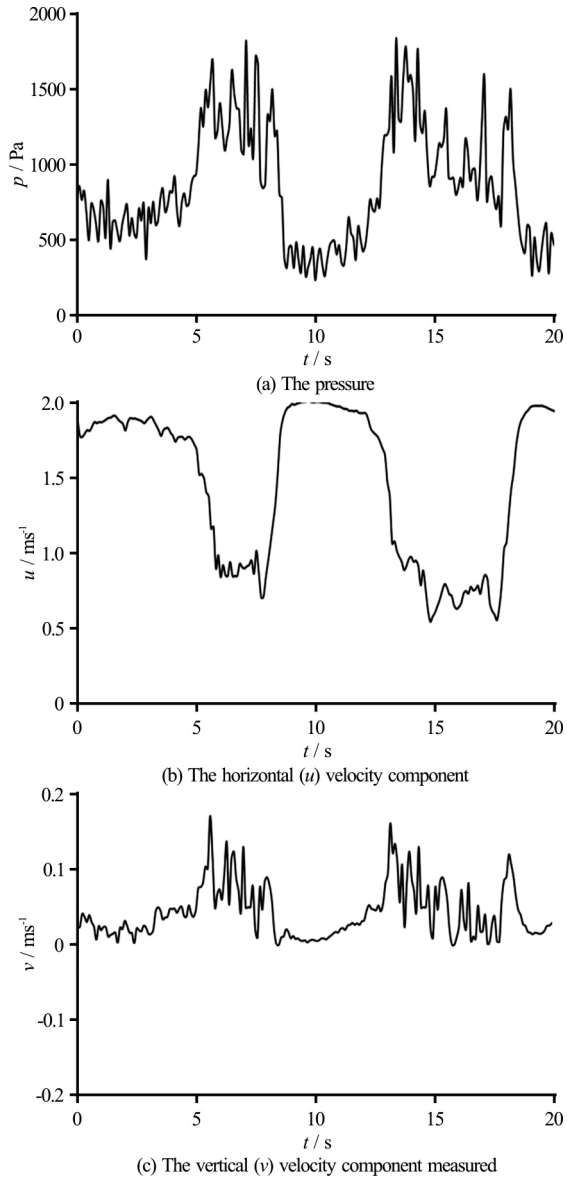

Fig. 13 Time series at the bottom under the hydraulic jump

Correlation coefficients can also be easily computed from SPH results. The correlation coefficient r is defined as

$$r = \frac{\sum_{i=1}^{n}\left[\left(x_{1_i} - \overline{x_1}\right)\left(x_{2_i} - \overline{x_2}\right)\right]}{\sum_{i=1}^{n}\left[\left(x_{1_i} - \overline{x_1}\right)^2\left(x_{2_i} - \overline{x_2}\right)^2\right]} \quad (4)$$

where x_1 and x_2 are two variables, respectively, while the bar denotes a time average. Figure 14 shows the correlation coefficient $r(p,u)$ at different locations downstream of the average position of the jump toe. It can be seen that pressures and streamwise velocities are strongly anti-correlated near the jump (i.e., lower pressures, and levels, occur when the streamwise velocity is higher, and viceversa), while they show a positive correlation downstream. The correlation coefficient $r(u,v)$ between the velocity components exhibits a similar behaviour.

This result is consistent with the oscillation between the B-jump (Figs. 11(a) and 11(c)) and the wave-jump (Figs. 11(b) and 11(d)) patterns.

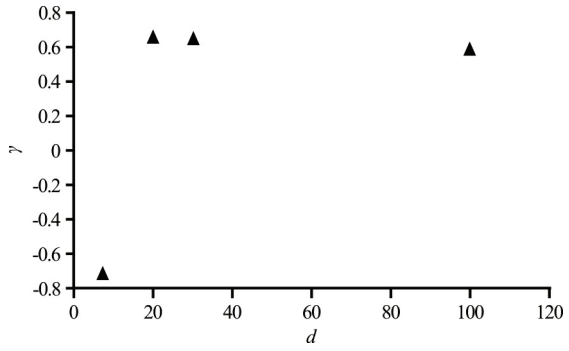

Fig. 14 Correlation coefficients between pressure and streamwise velocity component as a function of the distance d from the average toe position

4. Conclusions

The 2-D SPH model was applied to the modelling of the transition from supercritical to subcritical flow at an abrupt drop based on the laboratory experiments by[6]. Oscillating characteristics in the hydraulic jump are investigated and reproduced using a weakly-compressible XSPH scheme, together with either an algebraic mixing-length or a two-equation turbulence model to represent turbulent stresses: a sensitivity analysis was therefore performed on the influence of different turbulence model. Both turbulence models yield similar results, although the detailed comparison of the computed amplitude spectra with the measured ones shows that the mixing-length model predicts an oscillation frequency and amplitude which iscloser to the one obtained from the experimental data. However, the k-ε simulation allows one to obtain information on the turbulence characteristics in the two-phases of the oscillation, showing that the wave-jump phase exhibits a sub-surface turbulent layer which is more persistent than in the B-jump phase.

As observed experimentally by Mossa et al.[6], these numerical results show the existence of a peak at a similar frequency in the amplitude spectra of the time series of the surface elevations upstream and downstream of the jump, in the amplitude spectra of the pressure and in the amplitude spectra of the velocity components fluctuations measured under the hydraulic jump.

It is possible to conclude that the SPH numerical simulations yield results which are in qualitative and quantitative agreement with the experiments: hence SPH can be used as a reliable “numerical experiment” which allows one to get a better insight in the unsteady flow phenomenon, performing detailed evaluations which can be complicated to be obtained during laboratory experiments. For instance, the analysis of amplitude spectra, of the vorticity fields and of the correlation coefficients indicates that velocity components and pressure fluctuations, are strongly influenced by the oscillations between the B and wave jump types, and that a strong correlation exists among the velocity and vorticity fields and the pressure fluctuations even far downstream of the jump position.

References

[1] Pagliara S. Transition from supercritical to subcritical flow at an abrupt drop [J]. *Journal of Hydraulic Research*, 1992, 30(3): 428-432.

[2] Nebbia G. Su taluni fenomeni alternativi in correnti libere [J] *L'Energia Elettrica*, 1942, XIX(1): 1-10.

[3] Abdel Ghafar A., Mossa M., Petrillo A. Scour from flow downstream of a sluice gate after a horizontal apron [C]. *6th International Symposium on River Sedimentation-Management of Sediment-Philosophy, Aims, and Techniques*, New Delhi, India, 1995, 1069-1088.

[4] Mossa M. On the oscillating characteristics of hydraulic jumps [J]. *Journal of Hydraulic Research*, 1999, 37(4): 541-558.

[5] Wang H., Chanson H. Experimental study of turbulent fluctuations in hydraulic jumps [J]. *Journal of Hydraulic Engineering, ASCE*, 2015, 141(7): 04015010.

[6] Mossa M., Petrillo A., Chanson H. Tailwater level effects on flow conditions at an abrupt drop [J]. *Journal of Hydraulic Research*, 2003, 41(1): 39-51.

[7] Dalrymple R. A., Rogers B. D. Numerical modelling of waves with the SPH method [J]. *Coastal Engineering*, 2006, 53(2-3): 131-147.

[8] Capone T., Panizzo A., Monaghan J. J. SPH modelling of water waves generated by submarine landslides [J]. *Journal of Hydraulic Research*, 2010, 48(Suppl. 1): 80-84.

[9] De Padova D., Dalrymple R. A., Mossa M. Analysis of the artificial viscosity in the smoothed particle hydrodynamics modelling of regular waves [J]. *Journal of Hydraulic Research*, 2014, 52(6): 836-848.

[10] Espa P., Sibilla S., Gallati M. SPH simulations of a

vertical 2-D liquid jet introduced from the bottom of a free-surface rectangular tank [J]. *Advances Application Fluid Mechanics*, 2008, 3(2): 105-140.

[11] De Padova D., Mossa M., Sibilla S. et al. 3D SPH modelling of hydraulic jump in a very large channel [J]. *Journal of Hydraulic Research*, 2013, 51(2): 158-173.

[12] Jonsson P., Andreassona P., Hellström J. G. I. et al. Smoothed particle hydrodynamic simulation of hydraulic jump using periodic open boundaries [J]. *Applied Mathatical Modelling*, 2016, 40(19-20): 8391-8405.

[13] De Padova D., Mossa M., Sibilla S. SPH modelling of hydraulic jump oscillations at an abrupt drop [J]. *Water*, 2017, 90: 790-814.

[14] De Padova D., Mossa M., Sibilla S. SPH numerical investigation of characteristics of hydraulic jumps [J]. *Environmental Fluid Mechahics*, 2017, https://doi.org/10.1007/s10652-017-9566-4.

[15] De Padova D., Mossa M., Sibilla S. SPH numerical investigation of the velocity field and vorticity generation within a hydrofoil-induced spilling breaker [J]. *Environmental Fluid Mechanics*, 2016, 16(1): 267-287.

[16] Mossa M., Tolve U. Flow visualization in bubbly two-phase hydraulic jump [J]. *Journal of Fluids Engineering*, 1998, 120(1): 160-165.

[17] Mossa M. Discussion on "Relation of surface roller eddy formation and surface fluctuation in hydraulic jumps" by K. M. Mok [J]. *Journal of Hydraulic Research*, 2005, 43(5): 588-592.

[18] Mossa M., Petrillo A., Chanson H. Discussion on the "Tailwater level effects on flow conditions at an abrupt drop" [J]. *Journal of Hydraulic Research*, 2004, 43(2): 217-224.

[19] Mossa M. Experimental study of the flow field with spilling type breaking [J]. *Journal of Hydraulic Research*, 2008, 46(Suppl. 1): 81-86.

[20] Liu G. R., Liu M. B. Smoothed particle hydrodynamics: A meshfree particle methods [M]. Singapore: World Scientific, 2005.

[21] Monaghan J. J. Simulating free surface flows with SPH [J]. *Journal of Computational Physics*, 1992, 110(2): 399-406.

[22] Sibilla S. An algorithm to improve consistency in smoothed particle hydrodynamics [J]. *Computers and Fluids*, 2015, 118: 148-158.

[23] De Padova D., Mossa M., Sibilla S. Laboratory experiments and SPH modelling of hydraulic jumps [C]. *Proceedings of the 4th SPHERIC Workshop*, Nantes, France, 2009, 255-257.

[24] De Padova D., Mossa M., Sibilla S. et al. Hydraulic jump simulation by SPH [C]. *Proceedings of the 5th SPHERIC Workshop*, Manchester, UK, 2010, 50-55.

[25] Launder B. E., Spalding D. B. The numerical computation of turbulent flows [J]. *Computer Methods in Applied Mechanics and Engineering*, 1974, 3(2): 269-289.

[26] Dehnen W., Aly H. Improving convergence in smoothed particle hydrodynamics simulations without pairing instability [J]. *Monthly Notices of the Royal Astronomical Society*, 2012, 425(2): 1068-1082.

[27] De Padova D., Dalrymple R. A., Mossa M. et al. An analysis of SPH smoothing function modelling a regular breaking wave [C]. *Proceedings of the National Conference XXXI Convegno Nazionale di Idraulica e Costruzioni Idrauliche*, Perugia, Italy, 2008.